# Raman Spectroscopic Evidence of Tissue Restructuring in Heat-Induced Tissue Fusion

*Lei Su[1,2 ◊], Kristy L Cloyd[3,4,5 ◊], Shobhit Arya[1], Martin AB Hedegaard[3,4,6], Joseph AM Steele[3,4], Daniel S Elson[1,5], Molly M Stevens[3,4,5 *], George B Hanna[1*]*

[1]*Department of Surgery and Cancer, Imperial College London, St. Mary's Hospital, London W2 1NY, UK*

[2]*Department of Electrical Engineering & Electronics, University of Liverpool, Liverpool L69 3GJ, UK*

[3]*Department of Materials, Imperial College London, London SW7 2AZ, UK*

[4]*Department of Bioengineering, Imperial College London, London SW7 2AZ, UK*

[5]*Institute of Biomedical Engineering, Imperial College London, London SW7 2AZ, UK*

[6]*Department of Chemical Engineering, Biotechnology and Environmental Technology, University of Southern Denmark, Campusvej 55, 5230 Odense M*

[◊]*These authors contributed equally to this work*

[*] *m.stevens@imperial.ac.uk; g.hanna@imperial.ac.uk*

**Abstract:** Heat-induced tissue fusion via radio-frequency (RF) energy has gained wide acceptance clinically and here we present the first optical-Raman-spectroscopy study on tissue fusion samples *in vitro*. This study provides direct insights into tissue constituent and structural changes on the molecular level, exposing spectroscopic evidence for the loss of distinct collagen fibres rich tissue layers as well as the denaturing and restructuring of collagen crosslinks post RF fusion. These findings open the door for more advanced optical feedback-control methods and characterization during heat-induced tissue fusion, which will lead to new clinical applications of this promising technology.

**Key Words:** Raman spectroscopy, Raman imaging, tissue fusion, tissue diagnostics

## 1. Introduction:

Tissue sealing and reconnection are routine surgical procedures. Among other technologies, heat-induced tissue fusion using radio-frequency (RF) energy has attained wide acceptance. In surgery, RF based blood vessel sealing has been clinically approved [1, 2], e.g., the RF bipolar vessel sealer (LigaSure™, Covidien, USA). More recently, significant research efforts have been made to develop new fusion instruments for other tissue types, e.g. intestinal tissues during bowel anastomosis, to replace traditional hand suturing or stapling [3-5]. This technology exploits the heat-induced fusion of native tissues to achieve high-quality rapid tissue sealing without introducing any foreign materials, and thus, is expected to greatly reduce morbidity, mortality and cost.

The mechanism for heat-induced tissue fusion, particularly for blood vessel sealing, has been discussed in many studies [2, 4-6]. Heat-induced tissue fusion is believed to be the result of simultaneously applied heat and compression pressure (CP). Changes in collagen bonds within the fused tissue are thought to be pivotal to the strength of the resulting fusion. It is widely accepted that heat denatures collagen to a gel-like amalgam, which then forms strong bonds between neighbouring tissues [2][6]. The existing characterization and analysis, however, have been mainly made on either direct microscopic observation or mechanical strength testing. The lack of

understanding at the molecular and cellular levels has left several important questions in this field unresolved. Critically it is still unclear as how the collagen changes within the fused tissue during heat-induced RF tissue fusion and the precise mechanism for the formation of the strong seal. Answering these questions will provide a better understanding and knowledge of the intrinsic mechanisms for RF tissue fusion and also help to develop more effective control methods for RF fusion procedures. Furthermore, the main challenge in intestinal tissue anastomosis is achieving effective control over the delivered energy to form a successful fusion without causing excessive thermal tissue damage. This requires a better understanding of the fusion mechanism and more importantly, the development of effective feedback technologies to control the fusion procedure. Therefore, more advanced techniques are in great demand to study RF tissue fusion on the cellular and molecular levels.

Raman spectroscopy provides an attractive way of rapidly capturing the molecular environment of tissues without destroying or altering the samples . Raman micro-spectroscopy generates information-rich spectra which, when combined with chemometrics, provides powerful insight into the molecular diversity within heterogeneous biological samples [7-9]. Proteins have been studied extensively using Raman spectroscopy as information regarding the amino acids, amide bonds between them and their tertiary structure can be extracted and analysed [10, 11]. In particular, Raman spectroscopy has been used to identify changes within isolated animal collagen during thermal and chemical denaturing [12, 13]. These studies provide a molecular fingerprint to identify collagen and demonstrate the powerful ability of Raman spectroscopy to expose specific molecular changes within collagen. Additionally, it is possible to deconstruct individual contributors, such as collagen, from an overall tissue sample for characterisation and comparison [14]. By scanning across an area of interest, the individual Raman spectrum at each acquisition point can be combined to form a Raman map, which is similar to a microscopic image but with the ability to focus on certain chemical markers within the imaged area. The Raman map provides a direct observation of molecular distributions, such as that of collagen fibres, within a sampled area.

In this current study, for the first time, we demonstrate the use of Raman spectroscopy to characterize RF tissue fusion *in vitro*. We performed tissue fusion with two tissue types, namely porcine blood vessels and small intestines, and assessed the seal quality based on the mechanical strength of the seal given by burst pressure (BP) testing. Porcine blood vessels were used as RF tissue fusion of blood vessels is established and clinically approved. We then acquired the Raman spectra from fusion samples characterized as either having a strong seals or weak seals according to BP testing, and conducted Raman mapping across fusion regions. We investigated whether there was a correlation between the Raman results and the mechanical strength of the seals, and examined the differences at the molecular level. The Raman maps were compared with conventional histopathology microscopic results to assess whether they were superior in characterizing RF tissue fusion due to the rich molecular information contained in fused tissue Raman spectra.

**Materials and Methods:**

*Animal Tissue Preparation:*

Fresh porcine small bowels were obtained from a local abattoir, cut into 20-30 cm long segments, moistened with physiological saline and refrigerated at 4ºC for up to 30 hours (from the time of slaughter) until needed for fusion experiments. Prior to the fusion experiment, sufficiently long tissue samples were selected and immediately dissected into 5 cm long pieces for tissue fusion experiment. Prepared 5 cm samples were kept hydrated in sealed plastic sample bags with saline and used within 30 minutes. Porcine blood vessels were cleaned, cut into 6 cm

long pieces, and then frozen within 4 hours from the time the animal was slaughtered. The frozen tissues were kept at -70°C. Frozen blood vessel samples were only thawed at room temperature immediately before the tissue fusion experiment.

*RF Tissue Fusion:*

RF energy was used as the source for tissue heating in this study. The RF generator was an energy research tool prototype developed by Covidien (Boulder, Colorado), capable of delivering a programmable sinusoidal current from 0-7 A and a power from 0-350 W. An operating RF frequency of 472 kHz was chosen to avoid neuromuscular stimulation and electrocution. Two tissue sealing devices were used in our experiment: a commercially available LigaSure™ Impact (Covidien) for blood vessel sealing and an anastomosis prototype for small bowel sealing (Figure 1). Pre-written RF energy control algorithms were loaded into the RF generator using fusion software written in LabVIEW (National Instruments) so that the entire procedure could be automated. The algorithm was designed to control RF energy delivery to achieve tissue heating and the applied energy was controlled using feedback from the measured tissue impedance to maintain a specific variation in impedance with time.

(a) (b)

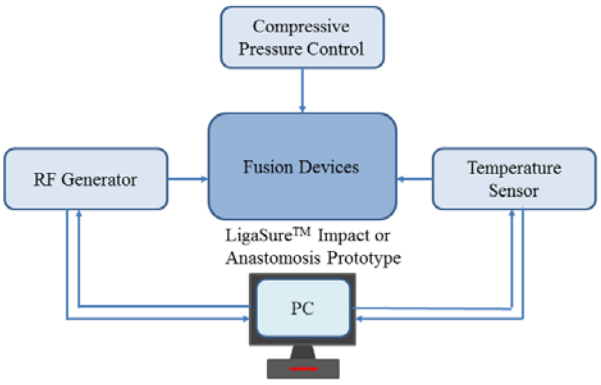


(c)

Figure 1. (a) LigaSure™ Impact fusion device for blood vessel sealing, (b) anastomosis prototype fusion device for small bowel sealing, and (c) RF tissue fusion setup.

During fusion, the tissue samples were clamped between the jaws of the fusion device. RF energy was supplied by the RF generator and applied to tissue samples via electrodes in jaws. The RF generator also continuously monitored both voltage and current delivered to the tissue. The varying tissue impedance was then obtained by using real-time voltage and current readouts. A compression spring in the handle of the LigaSure™ Impact device provided a constant pressure of ~0.3 MPa, and an air compressor was connected to the prototype, supplying a variable CP from 0–0.5 MPa. More than 200 tissue fusions were performed in the experiment.

*Temperature Measurements:*

Tissue temperature was measured using a fine (0.005 inch) tip Teflon-insulated J-type thermocouple (5TC-TT-J-36-36, Omega Engineering, Bridgeport, New Jersey). The thermocouple was inserted through slits present on the sealing device jaws and glued in place so that its tip protruded 0.25 mm above the electrode surface. In this way the thermocouple was in contact with the tissue surface without piercing it whilst remaining insulated from the electrode. The communication between the thermocouple and the computer was achieved through a National Instruments (NI) PXI-6289 DAQ board and a NI SCC-68 terminal block. The latter hosted four NI SCC-TC02 Thermocouple Signal Conditioning Modules. Each SCC-TC02 could drive one thermocouple and had individual signal conditioning modules with a 2 Hz low-pass filter, which filtered out the RF signal and eliminated the RF interference from the thermocouple readout.

There were in total more than 200 porcine small-bowel fusion temperature profiles recorded. The embedded thermocouple recorded a two stage evolution in tissue temperature evolution during fusion: a rapid increase in tissue temperature within a few seconds followed by a relatively stable plateau where the tissue temperature variation was within the range of ± 5°C. The tissue temperature was determined by the impedance control algorithm. A steep rising slope significantly reduces the duration of the whole procedure and a higher plateau temperature in the range between 60°C to 90°C ensures the necessary collagen denaturation in the tissue [2, 6], which is believed to be essential for a strong fusion. Plateau temperatures below 60°C may not lead to the denaturation of collagens, while excessive temperatures need to be avoided as they lead to permanent damage of the tissue or necrosis.

*Sample Preparation and Imaging*

Tissue samples were stored at -80°C, following fusion. Thawed samples were trimmed and embedded in optimal cutting temperature medium (OCT, Tissue-Tek, Sakura, Torrance, California) by flash freezing in isopentane at -160°C. The OCT blocks were sectioned on a cryostat at -20°C, cutting 15 µm sections for histology and Raman spectroscopy. Sections for histology were mounted on glass, washed with water to remove the OCT, and stained with haematoxylin and eosin (H&E). Sections for Raman analysis were mounted on $MgF_2$ slides, stored at 4°C, and imaged without further processing. Visualisation of the H&E-stained sections was performed under 4x magnification on an Olympus IX51 inverted light microscope, captured digitally and spliced together to allow visualisation of the entire field.

*Burst Pressure Measurements:*

The mechanical strength of the fused tissue was evaluated by a burst pressure (BP) testing system. This system consisted of a syringe pump, a pressure gauge, a sample injection needle and a surgical clamp to close the small bowel tissue. The main arm of a Y-splitter tubing system was connected to a water-filled syringe controlled by

the syringe pump. The other two split arms were connected to the pressure gauge and the sample injection needle, respectively. The surgical clamp sealed the other end of the piece of fused small bowel. The sample injection needle pierced the small bowel tissue to allow water to be injected into the sealed bowel without damaging the seal. After the initiation of the BP test, the syringe pump drove the water filled syringe to provide a flow rate of 20 mL/min, which constantly increased the pressure in the tubing system as well as in the fused tissue. Eventually the fused tissue burst at the fusion line, and the peak pressure was recorded as the BP.

More than 200 porcine small bowel segments were fused for BP testing. As we reported elsewhere [15], the BP, as an indication of the fusion mechanical strength, varied significantly with the change of CP during fusion. Tissue samples fused at CPs lower than 0.10 MPa displayed an average BP of ~10 mmHg, while samples fused at higher CPs (>0.10 MPa) showed an average BP of more than 20 mmHg. Increased burst pressures were observed at all CP values above 0.10 MPa. In order to study the correlation between seal strengths and corresponding Raman spectra, BP results were used as a guideline for planning the Raman experiments carried out in this work. Samples fused at three CPs (0, 0.2 and 0.3 MPa) with corresponding average BPs (10, 25, and 24 mmHg) were selected for analysis in order to understand the resulting differences in fusion strength. For blood vessel samples, a commercial LigaSure$^{TM}$ Impact fusion device was employed with a fixed value of ~0.3 MPa. The average BP for the blood vessels was above 100 mmHg, higher than for small bowel samples due to differences in the tissue and devices used.

*Raman Micro-spectroscopy:*

Tissue Raman maps were collected with a 785 nm laser, using a Renishaw InVia spectrometer connected to a Leica microscope as previously described [16]. Raman maps were collected over selected regions of interest with a step size of 75 µm in the x and y direction. At each point a spectrum was collected using five accumulations of five second scans covering the Raman shifts range of 620-1700 $cm^{-1}$. Samples were tested for no longer than 1 hour at room temperature and kept hydrated using saline.

Raman spectra were pre-processed for substrate background removal (baseline subtraction using weighted least squares) [17] and extended multiplicative scattering correction [18, 19]. For Raman mapping the N-FINDR spectral unmixing algorithm was used for each map independently as it searches the original input spectra, from the non-dimension reduced input matrix, for the most extreme spectra present and exposes these as endmembers. These endmembers were then identified based on their spectral features as pure contributing component of the tissue (in this study, the endmember corresponding to the collagen within the tissue was of interest). After the identification of each relevant endmember a Raman map was constructed with each pixel represented as a linear combination of the endmembers as previously described [22]. Each pixel thus contains an abundance value between 0 and 1 for the presence of each endmember within the pixel's spectrum [22]. All data analysis was performed in MatLab R2011a (The Mathworks, Natick, MA, Massachusetts) with in house written scripts in combination with the PLS_toolbox 7.0 (Eigenvector Research, Wenatchee, Washington).

**Results:**

*Raman Micro-spectroscopy Results:*

RF fused blood vessels and small bowel samples fused at different CPs were imaged using Raman spectroscopy. Raman maps were collected from selected regions within the tissue cross-sections including fused areas,

undisturbed and thus considered ‘healthy’ areas, and the interface between them. Raman maps of selected regions are shown for a fused porcine blood vessel at 0.3 MPa compression (Figure 2) and porcine blood vessels (Figure 3) fused (a) without compression, (b) with 0.2 MPa compression and (c) with 0.3 MPa compression. A white light micrograph showing the cross section of each tissue sample is shown in each figure (Figures 2 and 3, top left of the figure) with rectangular boxes highlighting the areas that were mapped by Raman. The three areas which were selected for mapping included (Figures 2,3 A) healthy tissue, (Figures 2,3 B) the interface between healthy and fused tissues and (Figures 3,4 C) fused tissues. The resulting Raman map and the endmember spectra identified in the sample and used to construct the Raman map are shown in Figures 2,3 A-C. All Raman maps shown were reconstructed from the two endmember as shown in spectra in each panel.

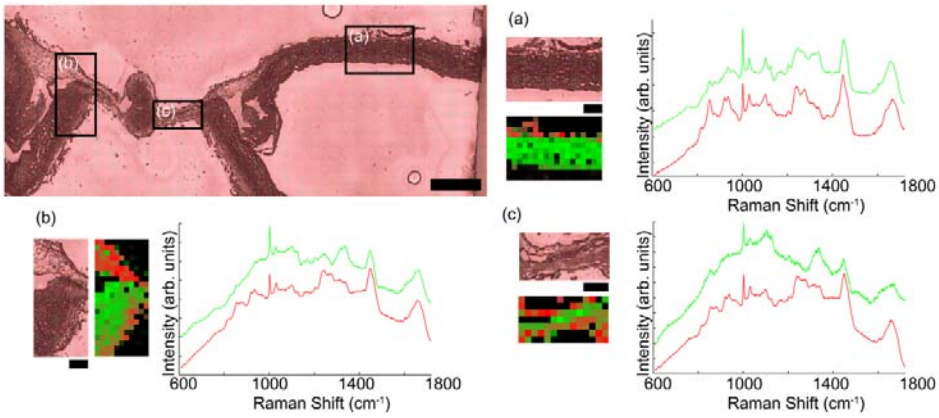


Figure 2. Raman spectroscopy maps collected from within a porcine blood vessel tissue at the locations indicated in the white light micrograph (shown in the top left, scale bar = 1 mm). Mapped regions included (a) healthy tissue, (b) interface between fused and healthy tissues and (c) fused tissue. White light images of each area selected for Raman mapping are shown in sections [a-c] (scale bar = 250 µm) together with their corresponding Raman map shown in the red, green and black images. The spectra included in [a-c] shows the collagen endmember spectrum in red with the intensity of the red colouring in the Raman maps corresponding to the presence of collagen within that pixel. The non-collagen rich tissue endmember spectrum is shown in green and the intensity of the colour green in the Raman map corresponds to the presence of non-collagen rich tissue within that pixel.

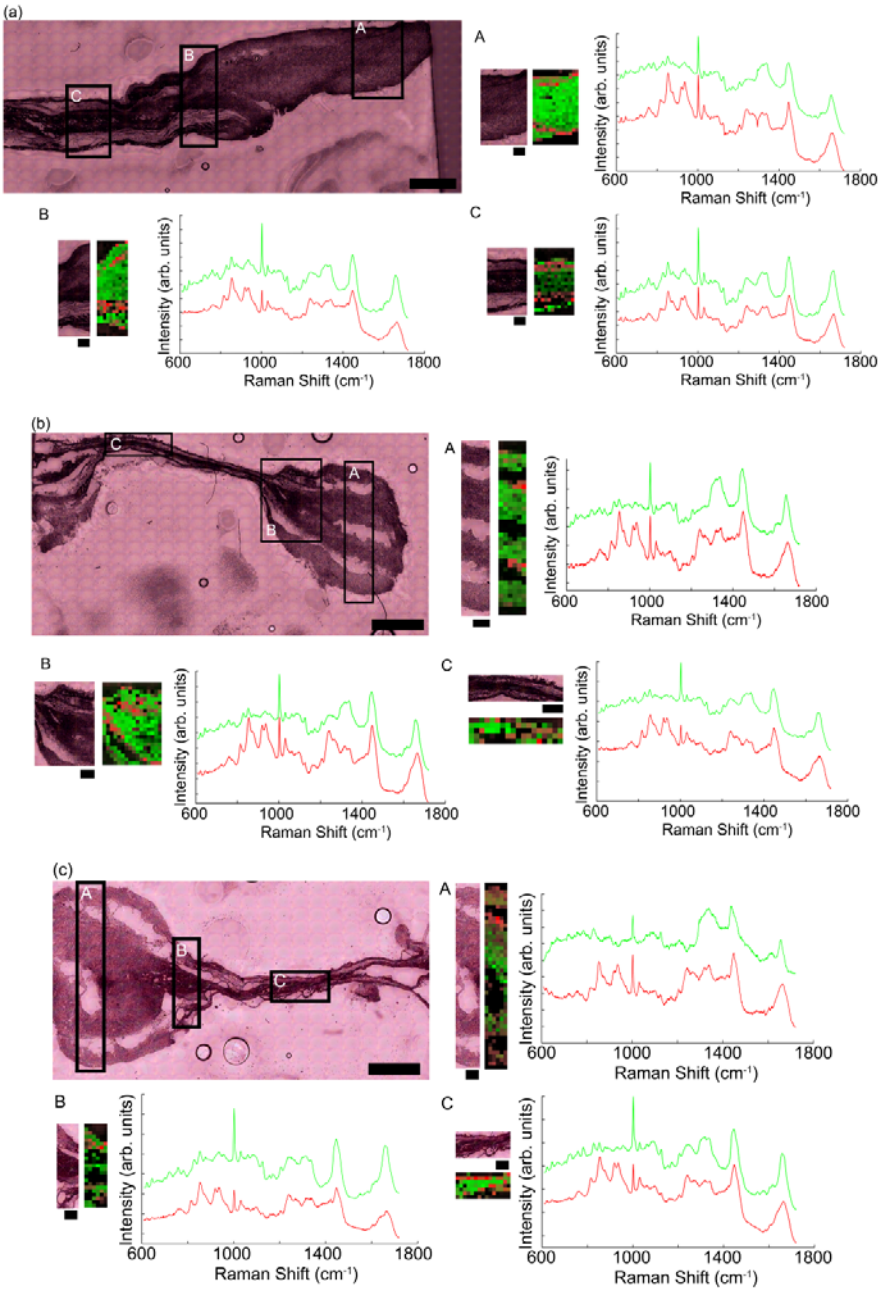


Figure 3. Raman maps collected over porcine bowel tissue selections (each shown in the top left white light micrograph, scale bar = 1 mm) with (a) no compression (b) compression at 0.2 MPa and (c) compression at 0.3 MPa. In each case mapped regions included [A] healthy, [B] interface between fused and healthy and [C] fused tissue. For each sub-region white light images of the area selected for Raman mapping are presented[A-C] (scale bar = 250 µm) together with their corresponding Raman maps shown in the red, green and black images. The spectra show the collagen endmember spectrum in red and the non-collagen rich endmember spectrum is shown

in green, and the intensities of red and green within the Raman maps are proportional to these signals.

The bottom spectrum (in red) representing the identified collagen endmember spectrum within the sample and the top spectrum (in green) presents the non-collagen rich tissue constituent. The collagen endmember spectrum identified by the N-finder algorithm in each map includes all the characteristic features previously reported in Raman spectroscopy studies of collagen and collagen rich tissues [20]. Specifically, Raman bands corresponding to C-C stretch of proline (855 $cm^{-1}$), C-C stretch of hydroxyproline (874 $cm^{-1}$), C-N stretch of proline (919 $cm^{-1}$), proline (1043 $cm^{-1}$), and Amide III (1245-1270 $cm^{-1}$) are notable [20]. The hydroxyproline and two proline peaks identified in these spectra are specifically Raman collagen assignments [20] confirming a collagen presence. The endmember spectrum which was identified to be non-collagen rich tissue included spectral features indicative of biological tissue including bands corresponding to cholesterols (699 $cm^{-1}$), phenylalanine (1003 $cm^{-1}$), C-H deformation of proteins (1262 $cm^{-1}$) and carbohydrates (1342 $cm^{-1}$), amide II (1480 $cm^{-1}$), and amide I (1663 $cm^{-1}$) [21].

The mean of all spectra collected from the healthy and fused areas of the blood vessel which underwent RF fusion and the bowel tissues which underwent RF fusion at 0 MPa, 0.2 MPa and 0.3MPa CP are shown in Figure 4. In both the blood vessel and the bowel tissues a shift in the peak maximum occurred in the 1663 $cm^{-1}$ Amide I band and a change in band shape was observed in the 1443 $cm^{-1}$ $C\text{-}H_2$ wag band compared with the fused mean spectrum from the healthy mean spectrum in each sample. Many peaks, including the 940 $cm^{-1}$ peak representing the protein alpha helix did not appear to change peak position or shape.

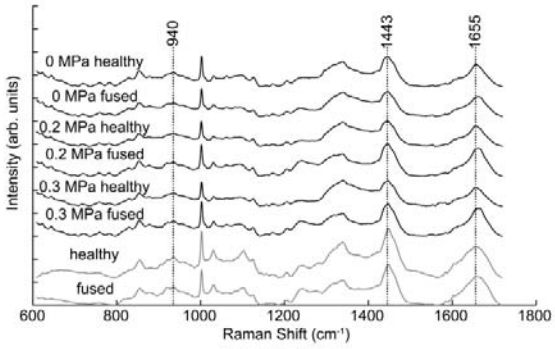


Figure 4. Mean Raman spectra of healthy and fused tissue areas mapped in porcine blood vessel and bowel tissue. Each spectrum labelled ‘healthy’ represents the mean of all collected spectra from an undisturbed cross section of the tissue. Each spectrum labelled ‘fused’ represents the mean of all collected spectra from the fused cross section of the tissue. Grey spectra were collected from porcine blood vessel tissue with and without radio frequency fusion as labeled. Spectra shown in black were collected from porcine bowel tissue with the corresponding compression pressure labelled (in the healthy spectrum, the pressure of the adjacent fused tissue is indicated in the label). Raman 940 $cm^{-1}$, 1443 $cm^{-1}$ and 1655 $cm^{-1}$ peaks are highlighted corresponding to the protein alpha helix, $CH_2$ wag, and the Amide I C-N-H stretch respectively.

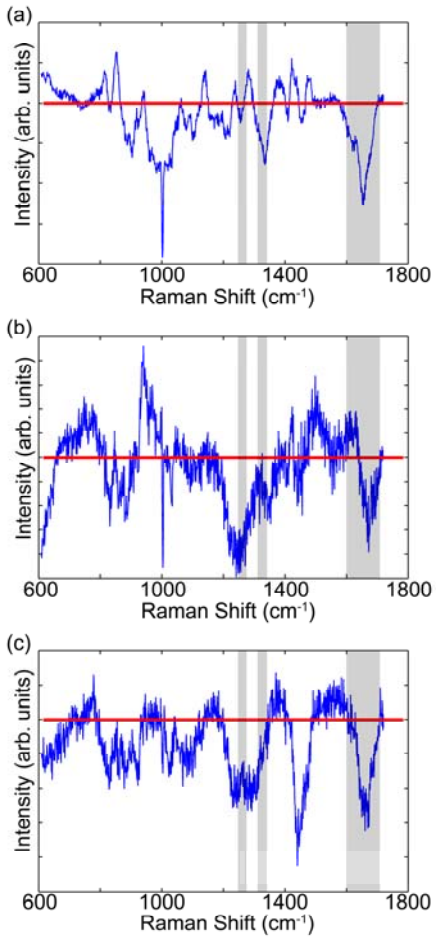


Figure 5. Difference Raman spectra of healthy - fused collagen rich tissue areas from (a) RF fused porcine blood vessel and (b) RF fused porcine bowel tissue without compression and (c) 0.20 MPa compression pressure. The red line indicates a zero difference. The 1313 $cm^{-1}$, 1324 $cm^{-1}$, 1252-1261 $cm^{-1}$ and 1600-1690 $cm^{-1}$ peaks are highlighted corresponding to the $CH_3CH_2$ twisting and wagging mode of collagen (respectively), amide III, and amide I (nonreducible collagen crosslinks at lower wavenumbers and reducible collagen crosslinks at higher wavenumbers) respectively.

Changes specifically in the collagen rich environments were investigated through a threshold analysis using the endmembers identified with the N-FINDR algorithm. Spectra showing an abundance value greater than 0.6 of the collagen rich endmember were selected and the means of these spectra were then calculated for each map. These means were then compared between healthy and fused areas to identify changes in the collagen environment due to fusion via a difference spectrum (Figure 5). Fused porcine blood vessel tissue showed the changes in the 1252-1261 $cm^{-1}$ peaks and a shift to lower wavenumbers in the 1447 $cm^{-1}$ peak. The 1600-1650 $cm^{-1}$ Amide I band

showed a shift to higher wavenumbers. For the bowel tissues, different changes were noted corresponding to different fusion CPs, however, only the samples which were fused with no compression and at 0.2 MPa compression were used for comparison as only these sample maps included more than three spectra which met the threshold requirements. The changes in the collagen rich spectra between fused and healthy areas were less pronounced in the porcine bowel tissue samples when compared to fused blood vessels. Bowel tissue fused at 0.2 MPa CP demonstrated similar but less distinct trends in the protein band shifts to the blood vessel results, specifically in the three broad protein bands, 1245-1270, 1445, and 1665 $cm^{-1}$ corresponding to the Amide 3, $CH_2$ bending and Amide 1 bands respectively. In bowel tissue fused without compression band shift trends included the 1245 and 1665 $cm^{-1}$ Amide III and Amide I band, respectively, however less dramatic shifts were seen in other protein bands (Figure 5).

*Histopathology Results:*

In Figure 6, the histopathology results are presented for a porcine blood vessel and porcine small bowels fused at different CPs. A reduction in the thickness and the loss of distinct tissue layering is observed in the fused porcine blood vessels as expected (Figure 6 (a)). A seal appears to have formed between the upper and lower small-bowel pieces for the porcine small bowel tissue sample fused at no compression pressure, as shown in Figure 6 (b) although the boundary between these two layers can still be seen. The three layers of small bowel tissue: serosa, submucosa and mucosa layers can be clearly identified and the delimitations between different layers are apparent. Although the tissue thickness was reduced at the mucosa layer, the tissue structure remains similar to the native tissue. Figure 6 (c) and (d) show porcine small-bowel samples fused at CPs of 0.2 and 0.3 MPa. Relative to Figure 6 (b), Figure 6 (c) and (d) display significant changes in the tissue structure resulting from the applied CP. The delimitation between submucosa and mucosa layers is less clear and the thickness of the mucosa layer has reduced considerably. Most importantly, a more homogeneous amalgam was formed by the upper and the lower mucosa layers in the centre of the fusion region, and the boundary between the upper and the lower mucosa layers has completely disappeared.

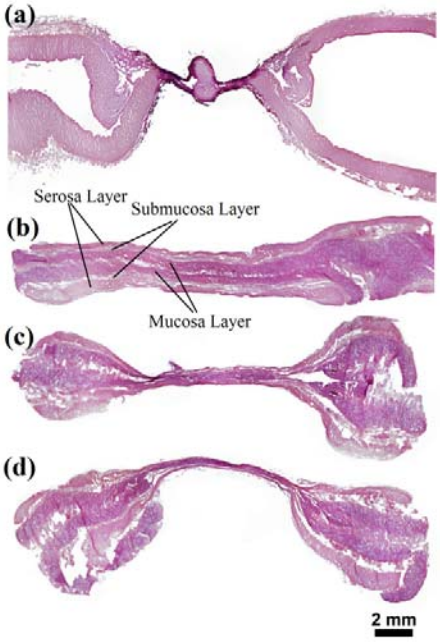

Figure 6. Histological sections of fusion samples for: (a) porcine blood vessel; (b) porcine small-bowel sample fused at 0 MPa; (c) porcine small-bowel sample fused at 0.2 MPa; and (d) porcine small-bowel sample fused at 0.3 MPa CP.

**Discussion:**

RF tissue fusion is a mature technology for blood-vessel sealing in modern surgery which holds great promise to reduce some of the critical complications in existing bowel anastomosis procedures including post-operative bleeding and leakage. Here we investigated the use of Raman spectroscopy to provide biomolecular insights into the restructuring which occurs during tissue fusion. Raman results were linked to optimal fusion parameters (CP in particular) obtained by comparing to the BP test results and histological sections.

Raman spectroscopy was conducted in order to explain the observed changes in mechanical strength shown in the BP measurement of fusions when CP was changed. Raman spectroscopy was applied to non-invasively image cross sections of healthy and fused tissue as shown in Figures 2 and 3. Applying N-FINDR spectral unmixing allowed for visualisation of the various bowel tissue layers by identification of the endmember spectra which are defined by the most extreme spectra present within the map [22]. The tissue layers identifiable through Raman spectroscopy correspond to those layers seen in the white light micrographs and in the histological sections by utilizing only two endmember spectra, one corresponding to a high collagen contribution and the other to non-collagen rich tissue. Raman spectroscopic maps were reconstructed from the two endmembers with endmember abundance plots overlaid and converted to red-green colour images based of the contribution of each endmember to each collected spectrum. The submucosal layer is clearly distinguished in each small intestinal cross section by its increased collagen content. During sectioning of the intestinal tissue, the shear force caused some separation of the healthy tissue sublayers (serosa, submucosa and mucosa). In Figure 3(a) A, the loss of the serosa is clearly visible in the white light micrograph and the corresponding Raman map. The collagen rich submucosa is located between the mucosa and serosa. The mucosa and serosa are shown to include many of the Raman spectral signatures of biological tissues including cells (DNA peaks included) and the extracellular matrix. Collagen Raman signature bands are found in the mucosa and serosa layers as well, however these layers appear to be less collagen rich with a greater cellular contribution corresponding to the known constituents of these tissue layers.

Previous reports have suggested that changes in collagen were significant in RF fusion [23, 24]. To further explore this we compared the collagen rich spectra from healthy and fused tissue. In order to perform this analysis the collagen rich spectra were identified as those having an abundance value greater than 0.6 for the collagen endmember spectrum found in each Raman map. The mean of all spectra which were identified to be predominantly collagen was then calculated and the healthy and fused tissue collagen was compared through the difference spectra of these collagen means as shown in Figure 5. This analysis was performed on both fused porcine blood vessels as well as fused porcine bowel tissue. The difference spectrum comparing areas of fusion to healthy tissue in blood vessels showed similar band shifts and thus biomolecular bond changes in two independent samples. These trends included the denaturing of collagen shown through the shift of the 1660 $cm^{-1}$ band to higher wavenumbers in the fused tissue area, also suggesting an increase in reducible crosslinks and a decrease of non-reducible cross links within the collagen [25]. Additionally a shift in the 1302 $cm^{-1}$ peak to higher wavenumbers has been previously reported in collagen thermal denaturing [13]. Changes in the 1313 $cm^{-1}$ and 1324 $cm^{-1}$ peaks signifying changes in the $CH_3CH_2$ twisting and wagging modes of collagen also

demonstrated a disruption to the native collagen [26, 27]. Lastly the apparent shift of the 1252-1261 $cm^{-1}$ peak's maximum intensity to lower wavenumbers also implicate that crosslinks may have been reduced or broken [28]. RF fusion of the porcine bowel tissue demonstrated less pronounced differences however fusion performed at 0.2 MPa compression pressure demonstrated many of the same changes, including shifts in the 1252-1261, 1313, 1324, 1443, and 1660 $cm^{-1}$ bands, as seen in the fused blood vessels, again indicating a denaturing of collagen and more specifically a decrease in non-reducible cross links and an increase in reducible cross links as seen in Figure 5(c).

Histopathology results show the fused tissue area to be thinner and lacking the tissue layers visible in healthy tissue. The merging and restructuring of the biochemical constituents of the tissue layers in the bowel tissue during RF tissue fusion with CP is also demonstrated in the Raman maps. At 0 MPa CP, the fused area is visibly thicker, and the tissue layers are still distinct as shown with the white light images and histology. The Raman map shows this again with the collagen rich layers remaining very distinct and encased by non-collagen rich layers as seen in Figure 3 (b and c). As the CP was increased to 0.2 MPa, the greatly reduced thickness of the fused area made it hard to visually distinguish whether the native tissue layers were still preserved post RF fusion. The Raman map indicated a collagen rich upper and lower layer in some areas of the fused region and less distinguishable collagen layering in other areas (Figure 3 (b)). Furthermore at 0.3 MPa CP there was no distinct layering of collagen rich and non-collagen rich regions within the fused tissue and collagen rich areas are found throughout the thin fused area. The collagen within the fused region of samples which underwent compression also demonstrated collagen cross linking modification and collagen amide bond modification which were not detected in tissue fused without compression as seen in the Raman results. When comparing these results to the burst pressure measurements, it is notable that both the 0.2 MPa and 0.3 MPa CP fused tissues showed median burst pressures of more than 20 mmHg. The correlation of higher burst pressures in the compressed fused tissue samples with less distinct tissue layering and a change in collagen crosslinking supports the hypothesis that collagen crosslinking modification via RF fusion plays an important role in the overall quality of the tissue fusion.

H&E histological stains of the porcine small intestinal tissue showed that fusion without compression produced a decrease in the tissue cross sectional thickness however the tissue layers and band structures appeared to remain much like that of the native state and produced a median burst pressure of less than 10 mmHg. RF fusion performed with accompanying compression showed a dramatic reduction in fused tissue thickness and significant changes in the tissue layers with the delimitation between the submucosa and mucosa layers becoming less distinguishable as seen in Figures 3 and 6. Additionally, the upper and lower mucosa of the fused tissue became indistinguishable from one another in the histological sections, white light micrographs and Raman maps. Fusion is therefore demonstrated by the unification of the mucosa during fusion along with the increase in burst pressure.

Tissue fused without compression appears to undergo some molecular restructuring as indicated in the mean plots (Figure 4) which may be expected due to exposure to higher temperatures. This molecular restructuring appears to be less collagen dependant as shown in the Raman difference plots in Figure 5(b) with the collagen difference spectrum highlighting fewer distinct band shifts in compressed tissue versus non compressed tissue. This may be attributed to more collagen bond restructuring with the additional mechanical pressure during fusion introduced with tissue compression.

Particular consideration to Raman spectral background changes was taken during the analysis of the Raman tissue maps as fibre and water content may alter the Raman background signal. A polynomial fit was used to

remove the background and spectra were normalised before comparing means directly or through difference spectra. Changes within the Raman spectral backgrounds were in line with expectations with the fused regions being more dense, less hydrated and less organised into distinct tissue layers. Some of the difference spectra were not considered (namely 0.3 MPa CP) as those tissue areas showed less than three spectra with an abundance value greater than 0.6 for the collagen rich endmembers. When comparing difference spectra it is also important to note that the collected Raman spectra are semi-quantitative thus general trends (peak shifts and shape changes) are important rather than absolute intensity differences. Future studies using a smaller mapping step sizes and/or a larger tissue section may be considered to improve upon these challenges.

**Conclusions:**

We have proposed and demonstrated for the first time the use of Raman spectroscopy to characterize fused tissues in RF heat-induced tissue fusion. We discovered that tissue restructuring, or more specifically tissue layer and collagen molecular restructuring in the fusion areas, seems to be a contributing mechanism for a strong fusion. These results suggest a decrease in non-reducible collagen crosslinks and an increase in reducible collagen crosslinks occur during fusion. These changes are associated with collagen undergoing heat treatment and this restructuring provides new insight into the effects of RF fusion on the biochemical changes in the native collagen. Additionally, the presence of compression pressure during fusion produced a difference in collagen restructuring. Tissues fused with compression showed an increase in collagen transformation while tissues fused without compression showed collagen changes associated with a heat treatment.

The correlation between the Raman maps and the histological maps supports the utilisation of Raman spectroscopy in the investigation of RF fusion quality and tissue restructuring. Raman spectroscopy allowed for highly spatially resolved mapping which provided biochemical information without suffering from hydration and tissue density changes between the healthy and fused tissue. The information rich nature of the collected Raman spectra combined with multivariate statistical analysis allowed the selection and comparison of the collagen content between tissue sections of interest. These abilities are of further interest when investigations of RF fusion and comparable techniques are compared in situ and in vivo. Raman microscopy has been demonstrated to be translatable into the clinical setting [29-31]. Thus the rapid, non-destructive, hydration and dehydration-compatible technique utilised in this study holds promise to further elicit information in the translation of the technique to bowel anastomoses.

Overall these insights are the first to demonstrate the previously suspected involvement of collagen in RF tissue fusion, both with and without concurrent compression, using Raman spectroscopy. These molecular insights help provide information on the transformation occurring due to RF fusion as well as inspiration for future investigations into optical feedback methods. In practice, these could be achieved by embedding a miniaturized fiber-optic Raman probe into the fusion device with associated real-time data analysis algorithms.

**Acknowledgements:**

This report is independent research funded by the Department of Health under the Health Technology Devices programme (HTD240). The views expressed in this publication are those of the authors and not necessarily those of the NHS or the Department of Health.

LS, SA and GBH receive funding from the UK Department of Health and Covidien$^{TM}$ under the Health Technology Devices programme (HTD240). MMS thanks ERC SIG grant Naturale for the funding of MMS and MABH. KLC was funded by the British Heart Foundation.

**Reference:**


[1] W. L. Newcomb, W. W. Hope, T. M. Schmelzer, J. J. Heath, H. J. Norton, A. E. Lincourt, B. T. Heniford, and D. A. Iannitti, "Comparison of blood vessel sealing among new electrosurgical and ultrasonic devices," *Surgical Endoscopy and Other Interventional Techniques,* vol. 23, pp. 90-96, Jan 2009.

[2] B. Sigel and M. R. Dunn, "MECHANISM OF BLOOD VESSEL CLOSURE BY HIGH FREQUENCY ELECTROCOAGULATION," *Surgery Gynecology and Obstetrics with International Abstracts of Surgery,* vol. 121, pp. 823-&, 1965 1965.

[3] H. Winter, C. Holmer, H. J. Buhr, G. Lindner, R. Lauster, M. Kraft, and J. P. Ritz, "Pilot study of bipolar radiofrequency-induced anastomotic thermofusion-exploration of therapy parameters ex vivo," *Int J Colorectal Dis,* vol. 25, pp. 129-33, Jan 2010.

[4] T. Floume, R. R. Syms, A. W. Darzi, and G. B. Hanna, "Real-time optical monitoring of radio-frequency tissue fusion by continuous wave transmission spectroscopy," *J Biomed Opt,* vol. 13, p. 064006, Nov-Dec 2008.

[5] T. Floume, R. R. Syms, A. W. Darzi, and G. B. Hanna, "Optical, thermal, and electrical monitoring of radio-frequency tissue modification," *J Biomed Opt,* vol. 15, p. 018003, Jan-Feb 2010.

[6] D. Foschi, P. Cellerino, F. Corsi, T. Taidelli, E. Morandi, A. Rizzi, and E. Trabucchi, "The mechanisms of blood vessel closure in humans by the application of ultrasonic energy," *Surgical Endoscopy and Other Interventional Techniques,* vol. 16, pp. 814-819, May 2002.

[7] C. Krafft, B. Dietzek, and J. Popp, "Raman and CARS microspectroscopy of cells and tissues," *Analyst,* vol. 134, pp. 1046-1057, 2009 2009.

[8] L. M. Moreira, L. Silveira, Jr., F. V. Santos, J. P. Lyon, R. Rocha, R. A. Zangaro, A. B. Villaverde, and M. T. T. Pacheco, "Raman spectroscopy: A powerful technique for biochemical analysis and diagnosis," *Spectroscopy-an International Journal,* vol. 22, pp. 1-19, 2008 2008.

[9] C. Krafft, A. A. Ramoji, C. Bielecki, N. Vogler, T. Meyer, D. Akimov, P. Rösch, M. Schmitt, B. Dietzek, and I. Petersen, "A comparative Raman and CARS imaging study of colon tissue," *Journal of biophotonics,* vol. 2, pp. 303-312, 2009.

[10] G. J. Thomas, "Raman spectroscopy of protein and nucleic acid assemblies," *Annual Review of Biophysics and Biomolecular Structure,* vol. 28, pp. 1-+, 1999 1999.

[11] J. L. Lippert, D. Tyminski, and P. J. Desmeules, "DETERMINATION OF SECONDARY STRUCTURE OF PROTEINS BY LASER RAMAN-SPECTROSCOPY," *Journal of the American Chemical Society,* vol. 98, pp. 7075-7080, 1976 1976.

[12] A. Alimova, R. Chakraverty, R. Muthukattil, S. Elder, A. Katz, V. Sriramoju, S. Lipper, and R. R. Alfano, "In vivo molecular evaluation of guinea pig skin incisions healing after surgical suture and laser tissue welding using Raman spectroscopy," *Journal of Photochemistry and Photobiology B-Biology,* vol. 96, pp. 178-183, Sep 4 2009.

[13] R. X. Dong, X. L. Yan, X. F. Pang, and S. G. Liu, "Temperature-dependent Raman spectra of collagen and DNA," *Spectrochimica Acta Part a-Molecular and Biomolecular Spectroscopy,* vol. 60, pp. 557-561, Feb 2004.

[14] N. Bergner, C. Krafft, K. D. Geiger, M. Kirsch, G. Schackert, and J. Popp, "Unsupervised unmixing of Raman microspectroscopic images for morphochemical analysis of non-dried brain tumor specimens," *Analytical and Bioanalytical Chemistry,* vol. 403, pp. 719-725, May 2012.

[15] S. Arya, N. Hadjievangelou, L. Su, H. Kudo, R. D. Goldin, A. W. Darzi, D. S. Elson, and G. B. Hanna, "Radiofrequency-induced small bowel thermofusion: an ex vivo study of intestinal seal adequacy using mechanical and imaging modalities," *Surg Endosc,* pp. 1-12, 2013.

[16] E. Gentleman, R. J. Swain, N. D. Evans, S. Boonrungsiman, G. Jell, M. D. Ball, T. A. V. Shean, M. L. Oyen, A. Porter, and M. M. Stevens, "Comparative materials differences revealed in engineered bone as a function of cell-specific differentiation," *Nature Materials,* vol. 8, pp. 763-770, Sep 2009.

[17] C. A. Lieber and A. Mahadevan-Jansen, "Automated method for subtraction of fluorescence from biological Raman spectra," *Applied Spectroscopy,* vol. 57, pp. 1363-1367, Nov 2003.

[18] P. Geladi, D. Macdougall, and H. Martens, "LINEARIZATION AND SCATTER-CORRECTION FOR NEAR-INFRARED REFLECTANCE SPECTRA OF MEAT," *Applied Spectroscopy,* vol. 39, pp. 491-500, 1985 1985.

[19] T. M. Hancewicz and C. Petty, "Quantitative analysis of vitamin A using Fourier transform Raman spectroscopy," *Spectrochimica Acta Part a-Molecular and Biomolecular Spectroscopy,* vol. 51, pp. 2193-2198, Nov 16 1995.

[20] B. G. Frushour and J. L. Koenig, "RAMAN-SCATTERING OF COLLAGEN, GELATIN, AND ELASTIN," *Biopolymers,* vol. 14, pp. 379-391, 1975 1975.

[21] Z. Movasaghi, S. Rehman, and I. U. Rehman, "Raman spectroscopy of biological tissues," *Applied Spectroscopy Reviews,* vol. 42, pp. 493-541, 2007 2007.

[22] M. Hedegaard, C. Matthaeus, S. Hassing, C. Krafft, M. Diem, and J. Popp, "Spectral unmixing and clustering algorithms for assessment of single cells by Raman microscopic imaging," *Theoretical Chemistry Accounts,* vol. 130, pp. 1249-1260, Dec 2011.

[23] J. R. Salameh, J. H. Schwartz, and D. A. Hildebrandt, "Can LigaSure seal and divide the small bowel?," *American Journal of Surgery,* vol. 191, pp. 791-793, Jun 2006.

[24] C. A. Shields, D. A. Schechter, P. Tetzlaff, A. L. Baily, S. Dycus, and N. Cosgriff, "Method for creating ideal tissue fusion in soft-tissue structures using radio frequency (RF) energy," *Surg Technol Int,* vol. 13, pp. 49-55, 2004 2004.

[25] C. P. Tarnowski, S. Stewart, K. Holder, L. Campbell-Clark, R. J. Thoma, A. K. Adams, M. A. Moore, and M. D. Morris, "Effects of treatment protocols and subcutaneous implantation on bovine pericardium: a Raman spectroscopy study," *J Biomed Opt,* vol. 8, pp. 179-184, Apr 2003.

[26] N. Stone, C. Kendall, J. Smith, P. Crow, and H. Barr, "Raman spectroscopy for identification of epithelial cancers," *Faraday Discussions,* vol. 126, pp. 141-157, 2004 2004.

[27] D. P. Lau, Z. W. Huang, H. Lui, D. W. Anderson, K. Berean, M. D. Morrison, L. Shen, and H. S. Zeng, "Raman spectroscopy for optical diagnosis in the larynx: Preliminary findings," *Lasers Surg Med,* vol. 37, pp. 192-200, Sep 2005.

[28] A. Carden, R. M. Rajachar, M. D. Morris, and D. H. Kohn, "Ultrastructural changes accompanying the mechanical deformation of bone tissue: A Raman imaging study," *Calcified Tissue International,* vol. 72, pp. 166-175, Feb 2003.

[29] E. B. Hanlon, R. Manoharan, T. W. Koo, K. E. Shafer, J. T. Motz, M. Fitzmaurice, J. R. Kramer, I. Itzkan, R. R. Dasari, and M. S. Feld, "Prospects for in vivo Raman spectroscopy," *Physics in Medicine and Biology,* vol. 45, pp. R1-R59, Feb 2000.

[30] S. Kaminaka, T. Ito, H. Yamazaki, E. Kohda, and H. Hamaguchi, "Near-infrared multichannel Raman spectroscopy toward real-time in vivo cancer diagnosis," *Journal of Raman Spectroscopy,* vol. 33, pp. 498-502, Jul 2002.

[31] M. G. Shim, L. Song, N. E. Marcon, and B. C. Wilson, "In vivo near-infrared Raman spectroscopy: Demonstration of feasibility during clinical gastrointestinal endoscopy," *Photochem Photobiol,* vol. 72, pp. 146-150, Jul 2000.